Nuclear Engineering and Technology 51 (2019) 1610–1615

Contents lists available at ScienceDirect

Nuclear Engineering and Technology

journal homepage: www.elsevier.com/locate/net

Original Article

Comparison of PET image quality using simultaneous PET/MR by attenuation correction with various MR pulse sequences

Chan Rok Park [a], Youngjin Lee [b, *]

[a] Department of Nuclear Medicine, Seoul National University Hospital, 101, Daehak-Ro, Jongno-Gu, Seoul, Republic of Korea
[b] Department of Radiological Science, Gachon University, 191, Hambakmoero, Yeonsu-gu, Incheon, Republic of Korea

ARTICLE INFO

Article history:
Received 13 February 2019
Received in revised form
29 March 2019
Accepted 8 April 2019
Available online 8 April 2019

Keywords:
Simultaneous PET/MR scanner
Attenuation correction with MR sequences
Quantitative evaluation of image quality

ABSTRACT

Positron emission tomography (PET)/magnetic resonance (MR) scanning has the advantage of less additional exposure to radiation than does PET/computed tomography (CT). In particular, MR based attenuation correction (MR AC) can greatly affect the image quality of PET and is frequently obtained using various MR sequences. Thus, the purpose of the current study was to quantitatively compare the image quality between MR non-AC (MR NAC) and MR AC in PET images with three MR sequences. Percent image uniformity (PIU), percent contrast recovery (PCR), and percent background variability (PBV) were estimated to evaluate the quality of PET images with MR AC. Based on the results of PIU, 15.2% increase in the average quality was observed for PET images with MR AC than for PET images with MR NAC. In addition, 28.6% and 71.1% improvement in the average results of PCR and PBV respectively, was observed for PET images with MR AC compared with that with MR NAC. Moreover, no significant difference was observed among the average values using three MR sequences. In conclusion, the current study demonstrated that PET with MR AC improved the image quality and can be help diagnosis in all MR sequence cases.

1. Introduction

In the early 2000s, the development of positron emission tomography (PET) in nuclear medicine played an important role in the diagnosis and treatment of cancer [1]. The principle of imaging using PET scanner is to detect two 511 keV gamma ray signals emitted from the body of the patient by a scintillator, and detecting signal acquires a gamma ray signal through a scintillator and photomultiplier tubes (PMTs).

However, the nuclear medicine image that expresses the distribution of the gamma ray signal causes signal attenuation and scatter while moving from the body of the patient to the scintillator. Therefore, scatter and attenuation correction (AC) procedures are essential for PET images. Several researchers have suggested that AC PET image is more effective than non-AC (NAC) PET in identification of the cancerous lesion and provides images with better quality [2,3]. *C. Bae* et al. evaluated the image quality with and without AC through an anthropomorphic torso phantom and patient study. The phantom was simulated to be a lesion by inserting a sphere of 3.4 cm and 1.8 cm in diameter. The spheres were not visible in NAC PET image. The lesion of patient was also not detectable in NAC PET image. Therefore.

NAC PET images might not represent the actual gamma ray distribution [2]. *K. R. Zasadny* et al. compared the primary lung tumor size in 21 patients with NAC PET and CT image. The researchers reported that the NAC PET image shows average overestimation of tumor size in 30% when compared to CT image. According to this paper, NAC PET images might result in distortion of tumor size and shape [3].

Prior to the development of PET/computed tomography (CT), the PET scanner corrected the region of attenuation using a radioactive isotope (^{68}Ge) to generate the AC PET image. This procedure was associated with increased patient discomfort due to prolonged duration of the examination. In addition, due to low number of photons, the image quality of PET was not excellent and it provided poor anatomical information. Currently, PET/CT using ionizing radiation has gained popularity and enables diagnosis of the anatomical structure and biochemical metabolism of the human body [4]. In addition, data from CT are also used to compensate for the attenuation of gamma rays, which inevitably occurs in nuclear medicine imaging [5]. PET image was obtained for PET image with

* Corresponding author.
E-mail address: yj20@gachon.ac.kr (Y. Lee).

https://doi.org/10.1016/j.net.2019.04.008

AC using Hounsfield unit (HU) acquired by CT with the linear attenuation coefficient of fitting to PET energy of 511 keV [6]. Thus, PET/CT is used commonly, as AC, using CT reduces the examination time and increases patient convenience [7]. *E. Kinahan* et al. reported that the efficiency of PET images with AC was confirmed using CT based scaling, segmentation, and hybrid segmentation/scaling method [8].

In recent years, PET/magnetic resonance (MR) has been developed that has advantages over the PET/CT imaging. More favorable soft tissue contrast can be obtained using MR, for example, spectroscopy, diffusion-weighted image. *G. Brix* et al. reported that effective dose per examination in PET/CT is approximately 7.0 mSv and 1.3 mSv for PET of 370 MBq ^{18}F-FDG and low dose CT protocol, respectively [9]. As a result, the technique reduces additional radiation exposure of the patient [10]. The Ingenuity TF PET/MR developed by Philips, in 2008, signified further advancement in PET/MR. However, the drawback of Ingenuity TF PET/MR is that simultaneous scanning of PET and MR is not possible [11]. PET and MR images are acquired sequentially, and subsequently fused automatically using the same method as that used for PET/CT. Favorable quality of images cannot be obtained using PET/MR scanner with PMTs due to disturbance in the movement of photons in the magnetic field [12]. In order to overcome these drawbacks, Biograph mMR (Siemens, Germany) conjugated avalanche photodiodes (APDs) to a PET scintillator. SIGNA PET/MR (GE, USA) scanner gained popularity by development of a new system using silicon PMTs (SiPMTs) [13,14]. Owing to development of the above-mentioned scanners, PET and MR images can be scanned simultaneously using one isocenter. Unlike PET/CT, the PET image with AC using the PET/MR apply for MR data. However, since the proton density of MR and the photon attenuation of PET are not physically related, use of the PET/CT AC method is inappropriate. In order to solve this problem, various MR AC techniques have been reported [15–18]. Currently, the sequences used for MR AC are the two-point T1-weighted Dixon and ultra short echo time (UTE) sequences. Tissue in the Dixon sequence is divided into four classifications (air, lung, fat, and soft tissue) to perform AC [15]. The Dixon sequence was corrected by applying the generalized autocalibrating partially parallel acquisition (GRAPPA) (MR $AC_{Dixon\text{-}GRAPPA}$) and controlled aliasing in parallel imaging results in higher acceleration (CAIPIRINHA) (MR $AC_{Dixon\text{-}CAIPI}$) algorithm for attenuation lesion [19]. UTE sequence (MR AC_{UTE}) is useful for AC of cortical bone [20]. Therefore, the purpose of the current study was to evaluate image quality of PET with and without MR AC in PET/MR scan. For this purpose, PET images were acquired with the reconstruction method using MR AC sequences (MR AC_{UTE}, MR $AC_{Dixon\text{-}CAIPI}$, and MR $AC_{Dixon\text{-}GRAPPA}$).

2. Materials and methods

2.1. MR AC sequences

There are three types of MR AC applied in PET/MR: MR AC_{UTE}, MR $AC_{Dixon\text{-}GRAPPA}$, and MR $AC_{Dixon\text{-}CAIPI}$. The characteristics of the MR AC sequence are as follows [21–25]. First of all, there is MR AC_{UTE}. MR AC_{UTE} sequence has an advantage to be able to distinguish cortical bone using multi echo time images. However, this sequence does not apply for the whole body scan since it takes several minutes to acquire MR AC_{UTE} data. That is why MR AC_{UTE} sequence is applied to dedicated lesion such as brain scan [21,22]. Second, MR $AC_{Dixon\text{-}GRAPPA}$ sequence is an extension technique the parallel imaging with localized sensitivities (PILS) and simultaneous acquisition of spatial harmonics (SMASH) methods. The strength of this sequence improves image quality with high SNR and good spatial resolution [23]. Since the scan time is approximately 20 s, patients who can not hold breath during acquisition of MR $AC_{Dixon\text{-}GRAPPA}$ sequence have a weak point that the artifact of the image may be occur. Finally, there is MR $AC_{Dixon\text{-}CAIPI}$ sequence, an extension sequence of the MR $AC_{Dixon\text{-}GRAPPA}$ sequence. This sequence is useful for patients who have difficulty breath hold because the scan time is short (10 s). The resolution can be improved, and the artifact can be reduced [24,25].

2.2. Image acquisition

An integrated 3.0T Biograph mMR (Siemens, Germany) PET/MR scanner was used. Table 1 shows the acquisition parameters. The phantom was filled with fluid (5 g NaCl per 1000 g water and 3.75 g $NiSO_4$) using Jaszczak phantom. Fig. 1 shows the settings for the experiment. The MR AC PET images were reconstructed with MR AC_{UTE}, MR $AC_{Dixon\text{-}CAIPI}$, and MR $AC_{Dixon\text{-}GRAPPA}$ sequences for 10 min.

2.3. Data analyses

PET images with magnetic resonance NAC (MR NAC), MR AC_{UTE}, MR $AC_{Dixon\text{-}CAIPI}$, and MR $AC_{Dixon\text{-}GRAPPA}$ were analyzed using AMIDE software. Each PET image was obtained followed by estimation of percent image uniformity (PIU), percent contrast recovery (PCR), and percent background variability (PBV) by setting the region of interests (ROIs).

The PIU is calculated as follows:

$$PIU\ (\%) = 100 \cdot \frac{S_{maximum} - S_{minimum}}{S_{maximum} + S_{minimum}} \quad (1)$$

where, $S_{maximum}$ is the maximum pixel value and $S_{minimum}$ is the minimum pixel value.

PCR is expressed as $Q_{H,\,j}$, which is calculated using the formula

$$Q_{H,j} = 100 \cdot \frac{\frac{C_{H,j}}{C_{B,j}} - 1}{\frac{a_H}{a_B} - 1} \quad (2)$$

where, the subscript j of Q represents the sphere of the inner diameter of j mm. $C_{H,\,j}$ represents the average count of j mm ROI, $C_{B,\,j}$ represents the 10 average background counts of j mm sphere. a_H/a_B is the ratio of hot sphere to background remaining 10:1.

The expression of the PBV is as follows:

$$N_j = 100 \cdot \frac{SD_j}{C_{B,j}} \quad (3)$$

where, the subscript j of N means j mm inner diameter. SD_j is the standard deviation of background ROI for sphere j mm. $C_{B,\,j}$ represents the mean count of the background ROI for sphere j mm. The ROI was set as the biggest of four spheres among the six spheres.

3. Results and discussion

The AC process is necessary to express the gamma ray emitted from the body of the patient, such as in nuclear medicine images. In the development of PET/MR, various MR sequences are applied to generate the PET image with AC. The purpose of the current study was to compare MR NAC PET images with MR AC PET images (MR AC_{UTE}, MR $AC_{Dixon\text{-}CAIPI}$, and MR $AC_{Dixon\text{-}GRAPPA}$).

Fig. 2 shows the PET phantom images, which apply for the MR NAC, MR AC_{UTE}, MR $AC_{Dixon\text{-}CAIPI}$, and MR $AC_{Dixon\text{-}GRAPPA}$, respectively. Fig. 3 shows the results of PIU. The PIU values were 84.4%, 99.7%, 99.8%, and 99.7% for MR NAC, MR AC_{UTE}, MR $AC_{Dixon\text{-}CAIPI}$, and

Table 1
Acquisition parameters of the current experiment.

MR Parameter				
MR sequence	TR (ms)	TE (ms)	FOV (mm)	Acquisition time (sec)
MR AC_{UTE}	11.94	0.07/2.46	300	118
MR $AC_{Dixon\text{-}CAIPI}$	4.26	1.24/2.47	500	8
MR $AC_{Dixon\text{-}GRAPPA}$	3.60	1.23/2.46	500	19
PET Parameter				
Acquisition time	10 min			
Reconstruction	3D OSEM (Iteration: 3, Subsets: 21)			
Post filter	Gaussian filter (6 mm)			
Matrix size	172 × 172			

※ AC: Attenuation correction, CAIPI: Controlled aliasing in parallel imaging results in higher acceleration, GRAPPA: Generalized autocalibrating partially parallel acquisition, UTE: Ultra short echo time.

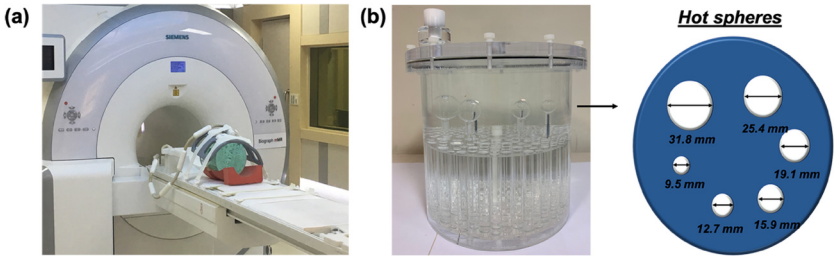

Fig. 1. Photos of (a) PET/MR system and (b) Jaszczak phantom containing six hot spheres.

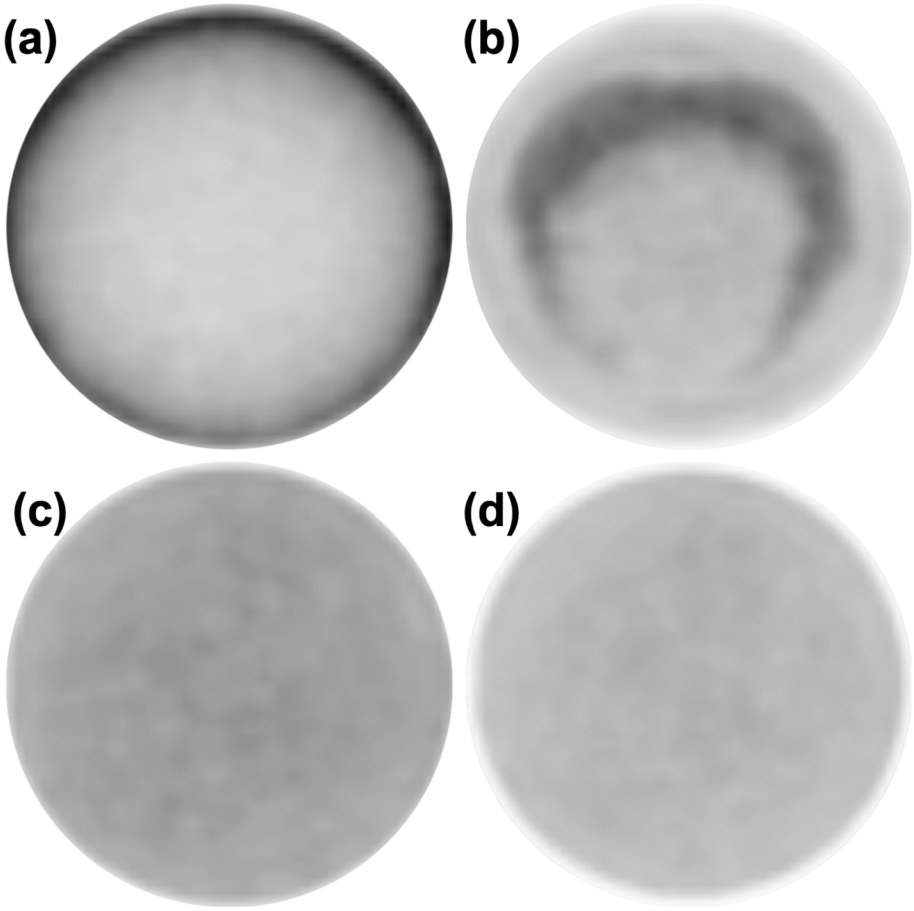

Fig. 2. PET phantom images applying for (a) MR NAC, (b) MR AC_{UTE}, (c) MR $AC_{Dixon\text{-}CAIPI}$, and (d) MR $AC_{Dixon\text{-}GRAPPA}$ sequence in PET/MR.

MR $AC_{Dixon\text{-}GRAPPA}$ PET, respectively. Compared to MR NAC PET, an increase was observed in MR AC_{UTE}, MR $AC_{Dixon\text{-}CAIPI}$, and MR $AC_{Dixon\text{-}GRAPPA}$ PET by 15.4%, 15.3%, and 15.3%, respectively. Fig. 4 shows the phantom images containing the four spheres obtained

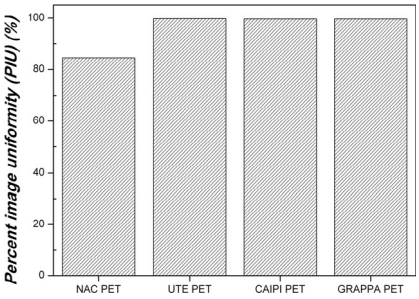

Fig. 3. Percent image uniformity (PIU) results between MR NAC and MR AC PET images, respectively (UTE PET: MR AC_{UTE} PET, CAIPI PET: MR $AC_{Dixon\text{-}CAIPI}$ PET, and GRAPPA PET: MR $AC_{Dixon\text{-}GRAPPA}$ PET).

using PET with MR NAC, MR AC_{UTE}, MR $AC_{Dixon\text{-}CAIPI}$, and MR $AC_{Dixon\text{-}GRAPPA}$ PET. Figs. 5 and 6 show the results of PCR and PBV for PET images with MR NAC and MR AC of the four spheres, respectively. The PCR of the PET images with MR NAC were 38.2%, 51.1%, 75.5%, and 73.8% at the sphere diameters of 15.9 mm, 19.1 mm, 25.4 mm, and 31.8 mm, respectively. The PCR of the PET images with MR AC was approximately 67.5%, 63.8%, 96.7%, and 99.8%, for each of the sphere diameters respectively. When the PET images were corrected using MR data for the attenuation lesion, PCR increased by 43.2%, 16.3%, 21.9%, and 26.1%, for each of the sphere diameters, respectively. The PBV of the PET images with MR NAC were 9.9%, 11.2%, 12.1%, and 14.4% at the sphere diameters of 15.9 mm, 19.1 mm, 25.4 mm, and 31.8 mm, for each of the sphere diameters, respectively. The average PBV of images with MR AC was 3.8%, 2.3%, 3.4%, and 4.0%, for each of the sphere diameters, respectively. The PBV of PET images with MR AC decreased by 62.1%, 79.1%, 70.6%, and 72.2%, respectively.

These results indicated that PET image with MR NAC can cause attenuation region according to our findings when compared with PET image with MR AC. In order to correct the attenuation region in PET/MR, MR pulse sequence is used to generate attenuation correction map with 3–4 segmentations of each tissues. The attenuated region is corrected by applying linear attenuation coefficients (LACs) corresponding to 511 keV to each tissue. *R. Boellaard* et al. compared MR AC PET image applying LACs using the national electrical manufacturers association (NEMA) image quality phantom according to three PET/MR scanner [26]. In addition, since there is no MR AC sequence to distinguish the bone, it is necessary to develop an MR AC sequence for the bone. In summary, MR data in PET/MR can provide more accurate diagnosis using various MR sequences and contrast agents that can be obtained from CT, the MR sequences play an important role in correcting the attenuation region of the photon emitted from the patient. *B. Zhang* et al. reported that attenuation correction is needed using MR sequences because photon attenuation occurs in the table and coil during PET/MR scan [27].

In addition, comparing the acquisition time of MR AC sequences, MR AC_{UTE}, MR $AC_{Dixon\text{-}CAIPI}$, and MR $AC_{Dixon\text{-}GRAPPA}$ require 118, 8, and 19 s, respectively. Since there was no significant difference in the quality of image between the three MR AC sequences, it is also important to consider the acquisition time required for clinical

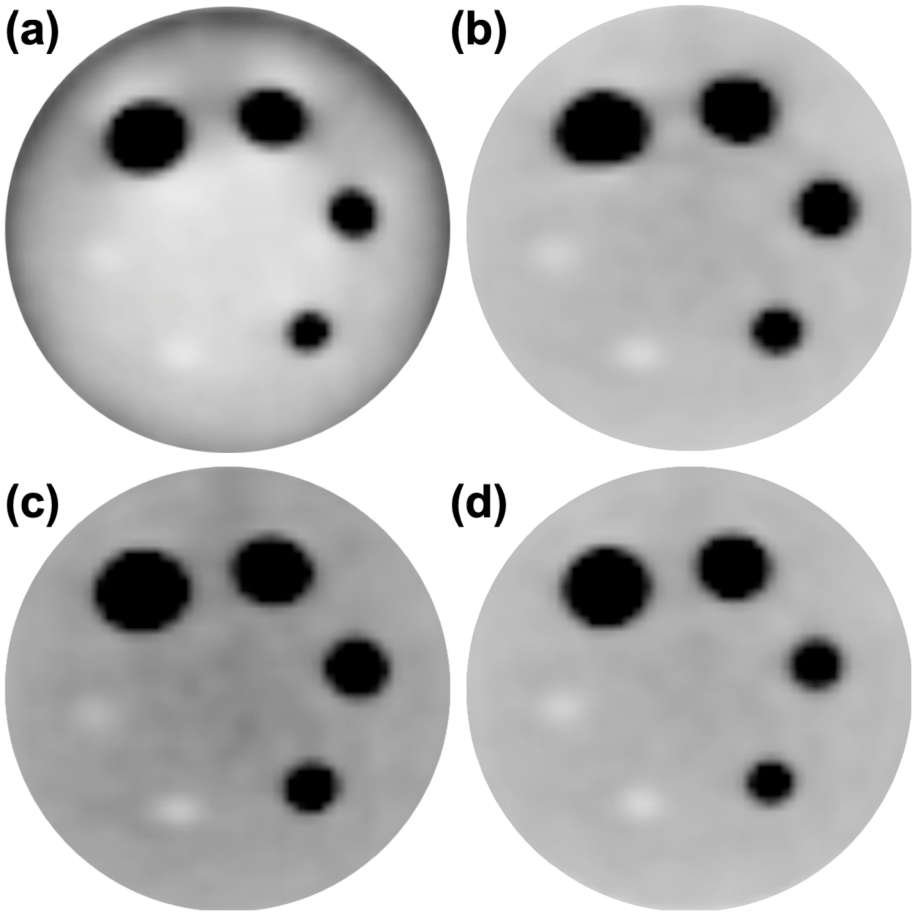

Fig. 4. PET phantom images using the four hot spheres applying for (a) MR NAC, (b) MR AC_{UTE}, (c) MR $AC_{Dixon\text{-}CAIPI}$, and (d) MR $AC_{Dixon\text{-}GRAPPA}$ sequence in PET/MR.

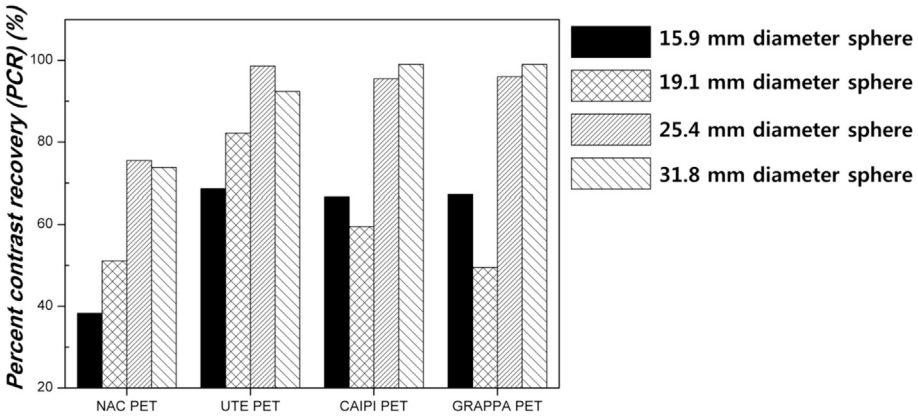

Fig. 5. Percent contrast recovery (PCR) results for MR NAC and MR AC PET images according to the spheres of four different diameters spheres (UTE PET: MR AC_{UTE} PET, CAIPI PET: MR $AC_{Dixon\text{-}CAIPI}$ PET, and GRAPPA PET: MR $AC_{Dixon\text{-}GRAPPA}$ PET).

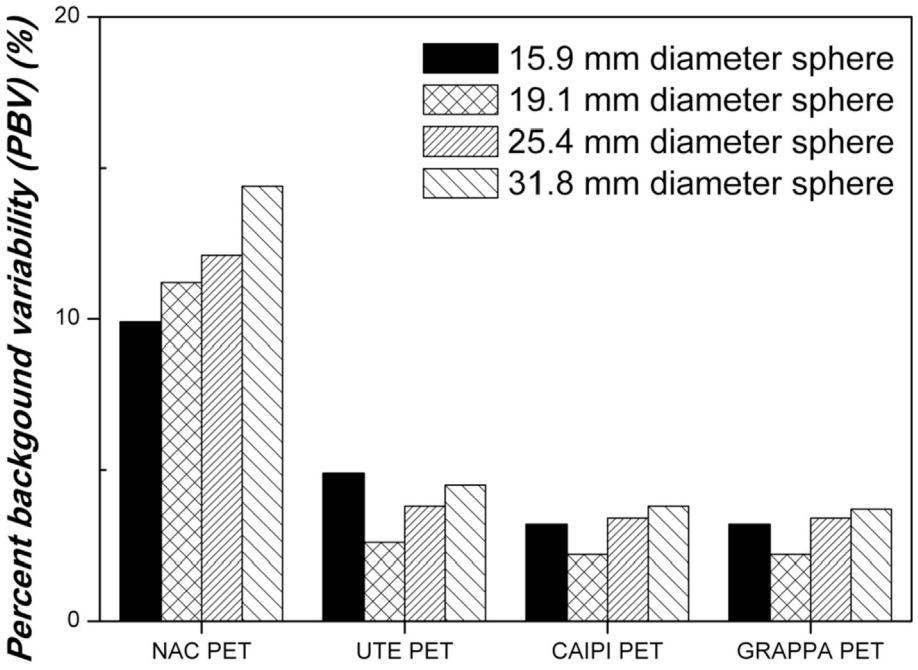

Fig. 6. Percent background variability (PBV) results for NAC and MR AC PET images according to the spheres of four different diameters spheres (UTE PET: MR AC_{UTE} PET, CAIPI PET: MR $AC_{Dixon\text{-}CAIPI}$ PET, and GRAPPA PET: MR $AC_{Dixon\text{-}GRAPPA}$ PET).

application in the patient. In case of MR $AC_{Dixon\text{-}CAIPI}$ and MR $AC_{Dixon\text{-}GRAPPA}$, acquisition time is short. Preventing degradation of image quality due to breath movements is possible by use of the two MR AC sequences. In addition, the Dixon sequence employs MR AC by segmenting tissues based on four classes (air, lung, soft tissue, and fat) for torso PET/MR scanning. Unfortunately, due to short T2 relaxation time of bone, distinguishing between air and bone is not feasible [28]. The UTE sequence consists of three segmentation compartments (air, soft tissue, and cortical bone). In particular, *V. Keereman* et al. suggested the usefulness of head MR AC when applying a UTE sequence that distinguishes the cortical bone [29].

Therefore, it may be confirmed that image quality of the PET with MR AC is superior to that of the PET with MR NAC. Based on the results of PIU, PCR, and PBV, it was confirmed that the image quality of MR AC was better than MR NAC. These results indicated that all PET images with MR AC have better uniformity and contrast recovery than PET images with MR NAC. In addition, background variability measured was also relatively low.

In this study, there are several limitations. First, additional study needs to be performed using the other standard phantom in nuclear medicine provided by NEMA. Second, this study can be performed with quantitative evaluation in AC PET images according to various MR pulse sequences through clinical examinations in the future research.

4. Conclusion

It may be confirmed that PET imaging with MR AC is superior to that of MR NAC. Therefore, it is necessary to reconstruct an excellent image quality by applying three types of MR sequences to correct the attenuated PET lesion during PET/MR.

Acknowledgment

The research was supported by the National Research Foundation of Korea (NRF-2016R1D1A1B03930357).

References

[1] D.W. Townsend, Multimodality imaging of structure and function, Phys. Med. Biol. 53 (2008) R1–R39.

[2] C. Bai, P.E. Kinahan, D. Brasse, C. Comtat, D.W. Townsend, C.C. Melizer, V. Vilemagne, M. Charron, M. Defrise, An Analytic Study of the effects of attenuation on tumor detection in whole-body PET oncology imaging, J. Nucl. Med. 44 (2003) 1855–1861.

[3] K.R. Zasadny, P.V. Kison, L.E. Quint, R.L. Wahl, Untreated lung cancer: quantification of systematic distortion of tumor size and shape on non-attenuation corrected 2-[fluorine-18]fluoro-2-deoxy-d-glucose PET scans, Radiology 201 (1996) 873–876.

[4] P. Ziai, M.R. Hayeri, A. Salei, A. Salavati, S. Houshmand, A. Alavi, Role of optimal quantification of FDG PET imaging in the clinical practice of radiology, Radiographics 36 (2016) 481–496.

[5] C. Buchbender, V. Hartung-Knemeyer, M. Forsting, G. Antoch, T.A. Heusner, Positron emission tomography (PET) attenuation correction artefacts in PET/CT and PET/MRI, Br. J. Radiol. 86 (2013). https://doi.org/10.1259/bjr.20120570.

[6] J.P.J. Carney, D.W. Townsend, V. Rappoport, B. Bendriem, Method for transforming CT images for attenuation correction in PET/CT imaging, Med. Phys. 33 (2006) 976–983.

[7] E. Kamel, T.F. Hany, C. Burger, V. Treyer, A.H.R. Lonn, G.K.V. Schulthess, A. Buck, CT vs ^{68}Ge attenuation correction in a combined PET/CT system: evaluation of the effect of lowering the CT tube current, Eur. J. Nucl. Med. 29 (2002) 346–350.

[8] P.E. Kinahan, D.W. Townsend, T. Beyer, Attenuation correction for a combined 3D PET/CT scanner, Med. Phys. 25 (1998) 2046–2053.

[9] G. Brix, U. Lechel, G. Glatting, S.I. Ziegler, W. Münzing, S.P. Müller, T. Beyer, Radiation exposure of patients undergoing whole-body dual-modality ^{18}F-FDG PET/CT examinations, J. Nucl. Med. 46 (2005) 608–613.

[10] G. Ronald, Z. Nan, C. James, S. Matthias, L. Ralf, V. Markus, S. Günter, R. Wolfgang, F. Hubertus, APD-based PET detector for simultaneous PET/MR imaging, Nucl. Instrum. Methods Phys. Res. 569 (2006) 301–305.

[11] H. Zaidi, N. Ojha, M. Morich, J. Griesmer, Z. Hu, P. Maniawski, O. Ratib, D. Izquierdo-Garcia, Z.A. Fayad, Design and performance evaluation of a whole-body ingenuity TF PET-MRI system, Phys. Med. Biol. 56 (2011) 3091–3106.

[12] Z. Hu, N. Ojha, S. Renisch, V. Schulz, I. Torres, A. Buhl, D. Pal, G. Muswick, J. Penatzer, T. Guo, P. Bönert, C. Tung, J. Kaste, M. Morich, T. Havens, P. Maniawski, W. Schäfer, R.W. Günther, G.A. Krombach, L. Shao, MR-based attenuation correction for a whole-body sequential PET/MR system, in: IEEE Nuclear Science Symp. Conf. Record, NSS/MIC, 2009. http://doi.org/10.1109/NSSMIC.2009.5401802.

[13] G. Delos, S. Fürst, B. Jakoby, R. Ladebeck, C. Ganter, S.G. Nekolla, M. Schwaiger, S.I. Ziegler, Performance measurements of the siemens mMR integrated whole-body PET/MR scanner, J. Nucl. Med. 52 (2011) 1–9.

[14] A.M. Grant, M.M. Khalighi, S.H. Maramraju, G. Delso, C.S. Levin, NEMA NU 2-2012 performance studies for the SIPM-based ToF-PET component of the ge signa PET/MR system, Med. Phys. 43 (2016) 2334–2343.

[15] V. Schulz, I. Torres-Espallardo, S. Renisch, Z. Hu, N. Ojha, P. Börnert, M. Perkuhn, T. Niendorf, W.M. Schäfer, H. Brockmann, T. Krohn, A. Buhl, R.W. Günther, F.M. Mottaghy, G.A. Krombach, Automatic, three-segment, MR-based attenuation correction for whole-body PET/MR data, Eur. J. Nucl. Med. Mol. Imag. 38 (2011) 138–152.

[16] A. Martinez-Möller, M. Souvatzoglou, G. Delso, R.A. Bundschuh, C. Chefd'hotel, S.I. Ziegler, N. Navab, M. Schwaiger, S.G. Nekolla, Tissue classification as a potential approach for attenuation correction in whole-body PET/MRI: evaluation with PET/CT data, J. Nucl. Med. 50 (2009) 520–526.

[17] M. Hofmann, F. Steinke, V. Scheel, G. Charpiat, J. Farquhar, P. Aschoff, M. Brady, B. Schölkopf, B.J. Pichler, MRI-based attenuation correction for PET/MRI: a novel approach combibing pattern recognition and atlas registration, J. Nucl. Med. 49 (2008) 1875–1883.

[18] M. Hofmann, B. Pichler, B. Schölkopf, T. Beyer, Towards quantitative PET/MRI: a review of MR-based attenuation correction techniques, Eur. J. Nucl. Med. Imag. 36 (2009) S93–S104.

[19] C.R. Park, Y. Lee, H. Yang, Attenuation effect of PET images with and without the magnetic resonance breast coil using various MR attenuation correction sequences, Jpn. Mag. 23 (2018) 375–380.

[20] I.L.H. Reichert, M.D. Robson, P.D. Gatehouse, T. He, K.E. Chappell, J. Holmes, S. Girgis, G.M. Bydder, Magnetic resonance imaging of cortical bone with ultrashort TE pulse sequences, J. Magn. Reson. Imag. 23 (2005) 611–618.

[21] A. Waldman, J.H. Rees, C.S. Brock, M.D. Robson, P.D. Gatehouse, G.M. Bydder, MRI of the brain with ultra-short echo-time pulse sequences, Neuroradiology 45 (2003) 887–892.

[22] M.D. Robson, G.M. Bydder, Clinical ultrashort echo time imaging of bone and other connective tissues, NMR Biomed. 19 (2006) 768–780.

[23] M.A. Griswold, P.M. Jakob, R.M. Heidemann, M. Nittka, V. Jellus, J. Wang, B. Kiefer, A. Hasse, Generalized autocalibrating partially parallel acquisitions (GRAPPA), Magn. Reson. Med. 47 (2002) 1202–1210.

[24] F.A. Breuer, M. Blaimer, M.F. Mueller, N. Seiberlich, R.M. Heidemann, M.A. Griswold, P.M. Jakob, Controlled aliasing in volumetric parallel imaging (2D CAIPIRINHA), Magn. Reson. Med. 55 (2006) 549–556.

[25] F.A. Breuer, M. Blaimer, R.M. Heidemann, M.F. Mueller, M.A. Griswold, P.M. Jakob, Controlled aliasing in parallel imaging results in higher acceleration (CAIPIRINHA) for multi-slice imaging, Magn. Reson. Med. 53 (2005) 684–691.

[26] R. Boellaard, I. Rausch, T. Beyer, G. Delso, M. Yaqub, H.H. Quick, B. Sattler, Quality control for quantitative multicenter whole-body PET/MR studies: a NEMA image quality phantom study with three current PET/MR systems, Med. Phys. 42 (2015) 5961–5969.

[27] B. Zhang, D. Pal, Z. Hu, N. Ojha, T. Guo, G. Muswick, C. Tung, J. Kaste, Attenuation correction for MR table and coils for a sequential PET/MR system, in: IEEE Nuclear Science Symp. Conf. Record, NSS/MIC, 2009. http://doi.org/10.1109/NSSMIC.2009.5401737.

[28] Y. Berker, J. Franke, A. salomon, M. Palmowski, H.C.W. Donker, Y. Temur, F.M. Mottaghy, C. kuhl, D.I. Garcia, Z.A. Fayad, F. Kiessling, MRI-based attenuation correction for hybrid PET/MRI systems: a 4-class tissue segmentation technique using a combined ultrashort-echo-time/dixon MRI sequence, J. Nucl. Med. 53 (2012) 796–804.

[29] V. Keereman, Y. Fierens, T. Broux, Y.D. Deene, M. Lonneux, S. Vandenberghe, MRI-based attenuation correction for PET/MRI using ultrashort echo time sequences, J. Nucl. Med. 51 (2010) 812–818.